A stable ultrastructural pattern despite variable cell size in *Lithothamnion corallioides*

Valentina Alice Bracchi[1], Giulia Piazza[1], Daniela Basso[1]

[1]Department of Earth and Environmental Sciences, University of Milano-Bicocca, Milan, 20126, Italy
Correspondence to: Valentina A. Bracchi (valentina.bracchi@unimib.it)

Abstract. Recent advances on the mechanism and pattern of calcification in coralline algae lead to contradictory conclusions.
10   Coralline calcification appears biologically induced, as suggested by the dependency of its elemental composition on environmental variables. However, evidence of a biologically controlled calcification process, resulting in distinctive patterns at the scale of family, was also observed. To clarify the matter, five collections of *Lithothamnion corallioides* from the Atlantic Ocean and the Mediterranean Sea, across a wide depth range (12-66 m) have been analyzed for morphology, anatomy, and cell wall crystal patterns of both perithallial and epithallial cells, to detect possible ultrastructural changes. *L. corallioides*
15   shows the alternation of tiers of short-squared and long-ovoid/rectangular cells along the perithallus, forming a typical banding. The perithallial cell length decreases according to water depth and growth-rate, whereas diameter remains constant. Our observations confirm that both epithallial and perithallial cells show primary (PW) and secondary (SW) calcite walls. Rectangular tiles, with the long axis parallel to the cell membrane forming a multi-layered structure, characterize the PW. Flattened squared bricks characterize the SW with roundish outlines enveloping the cell and showing a zigzag pattern. Long
20   and short cells have different thickness of PW and SW, with a thicker SW and PW in short cells. Epithallial cells are one up to three flared cells, with the same shape of the PW and SW crystals. Despite the diverse seafloor environments and the variable *L. corallioides* growth-rate, the cell walls maintain a consistent ultrastructural pattern, with unaffected crystal shape and arrangement. A comparison with two congeneric species, *L. minervae* and *L. valens*, showed similar ultrastructural patterns in SW, but evident differences in the PW crystal shape. Our observations point to a biological control rather than an induction of
25   the calcification process in coralline algae and suggest a possible new morphological diagnostic tool for species identification, with relevant importance for paleontological application. Finally, secondary calcite, in form of dogtooth crystals that fill the cell lumen, has been observed. It represents a form of early alteration in living collections which can have implications in the reliability of climate and paleoclimate studies based on the geochemistry techniques.

1 Introduction

30   The subclass Corallinophycidae is spread globally and comprises the crustose coralline algae (CCA), important Mg-calcite calcifiers and habitat builders of rhodolith beds, temperate algal reefs and tropical coralgal reefs (Cabioch and Giraud, 1986;

Adey, 1986; Ries, 2006; Caragnano et al., 2009; Bracchi et al., 2014, 2016). The complex calcifying process in CCA takes place during their whole life span and involves the entire organism. For this reason, corallines bear witness to past benthic primary production by macroalgae with an excellent fossil record (Basso et al., 2007; Bracchi et al., 2014, 2016; Ragazzola et al., 2020).

Rhodoliths are unattached nodules formed mostly by CCA. Among them, free-living unattached branches usually characterize maerl beds in the NE Atlantic Ocean (Henrich et al., 1995; Birkett et al., 1998; Peña and Bárbara, 2008, 2009; Peña et al., 2014) and in the Mediterranean Sea (Huvé, 1956; Jacquotte, 1962; Gambi et al., 2009; Agnesi et al., 2011; Savini et al., 2012; Basso et al., 2017).

In both geographical settings, the most common species are *Lithothamnion corallioides* (P.Crouan and H.Crouan) P.Crouan and H.Crouan 1867 and *Phymatolithon calcareum* (Pallas) Adey and McKibbin (1970) (Adey and McKibbin, 1970) (Basso et al., 2017; Hernandez-Kantun et al., 2017).

L. corallioides is distributed between the Canary Islands, at roughly 28°N, and Scotland, at about 58°N (Irvine and Chamberlain, 1994; Wilson et al., 2004), and it is considered one of the most suitable species for paleoclimate reconstruction (Foster, 2001). This species usually forms twig-like structures, brown to pink or purplish, often sterile, with branch diameters typically in the range 1-2 mm, with knob-like apices (Irvine and Chamberlain, 1994). Primary production, respiration, and calcification of *L. corallioides* are strongly influenced by seasonality, because of the oscillations of temperature and irradiance levels (Adey and Mc Kibbin, 1970; Potin et al., 1990; Martin et al., 2006). *L. corallioides* shows a favorable response to temperature increase, reaching its maximum primary production during summer (Adey and Mc Kibbin, 1970; Potin et al., 1990). *L. corallioides* minimum survival temperature is between 2°C and 5°C, while the optimal growth is observed between 13°C (Adey and McKibbin, 1970) and 14°C (Blake and Maggs, 2003). In longitudinal sections, the periodical change in growth-rate, due to the alternation of seasons, generates perithallus banding in *Lithothamnion* species, as in the long protuberances of *L. corallioides*. It results in an evident alternation of tiers of thick-walled, generally short cells versus thin-walled long cells along the main axis of perithallus growth (Basso, 1995; Basso et al., 1997; Kamenos and Law, 2010, Burdett et al., 2011). The banding has been interpreted as the visible result of the effect of the environment (primarily temperature) on algal growth at different time scales (day, month) (Halfar et al., 2000; Foster, 2001). Alternatively, banding would represent the regular shift between tiers of cells possessing different wall structure (Nash et al., 2019).

In general, the calcifying process of CCA has been described as the deposition of tangential calcite needles in the outer part of the cell wall (interstitial matrix), followed by the formation of radial needles in the cell frame itself in contact with the plasmalemma. The polysaccharide and fibrillary matrix control both processes (Giraud and Cabioch, 1976; Irvine and Chamberlain, 1994; Adey, 1998; de Cervalho et al., 2017). In *L. corallioides*, calcification has been described as composed of tangential rod-shaped crystals in the primary wall (PW) and perpendicular fan-like rods in the secondary wall (SW) (Giraud and Cabioch, 1976). Borowitzka (1984, 1989) proposed that coralline algae have semi-organized calcification, suggesting that their calcification is biologically controlled, as also indicated by Cabioch and Giraud (1986), rather than induced, as more recently supported by de Cervalho et al. (2017) and Nash et al. (2019). Cell wall ultrastructures are recognized as a valuable

tool to define the phenotypic expression of genotypic information (Auer and Piller, 2020). The compelling evidence of a biological control over calcification in coralline algae was provided by the identification of family-specific cell wall ultrastructures. Epithallial cells in the genus *Lithothamnion* show crystal units as thin rectangular blocks (Auer and Piller, 2020). Seasonality, including seawater temperature oscillations and photoperiod, is considered one of the main factors affecting

70 the growth-rate and the biomineralization process (Steller et al., 2007; Kamenos and Law, 2010; Vásquez-Elizondo and Enríquez, 2017), which may influence the ultrastructure pattern.

The identification of CCA in present-day integrative taxonomy is based on genetic methods coupling with the morphological description and measurement of diagnostic features. Species identification in the fossil record is, on the contrary, merely based on the preservation of morphological taxonomic characters. Consequently, the identification of valuable morphological

75 characters as a tool for the definition of the paleontological species represents an important challenge. CCA are well represented in the fossil record and *L. corallioides* has been reported in the Pliocene of Spain (Aguirre et al., 2012) and in the Pleistocene of Southern Italy (Bracchi et al., 2014).

This study is aimed at describing the ultrastructural mineralogical features of *L. corallioides* from different geographic settings (northeastern Atlantic Ocean and Mediterranean Sea) and across a wide bathymetric interval (12-66 m) to test if the

80 ultrastructural pattern preserves under different environmental conditions and can be considered as an evident sign of biologically-controlled mineralogical process. Moreover, the identification of specific ultrastructural pattern could be considered as a valuable tool for species identification to be used also in paleobiology. *L. corallioides* has been targeted because of its wide distribution, both geographically and bathymetrically, and its occurrence in the fossil record.

2 Materials and methods

85 For this study, we considered five collections (Fig. 1, Tab. 1), from two different geographic settings: the Atlantic Ocean and the Western Mediterranean Sea, sampled by scuba-diver or grab at different depth ranging from 12 m for Morlaix Bay (France) down to 66 m (Pontine Islands, Italy). Table 1 reports location and date of sampling. All specimens have been collected alive. To highlight possible ultrastructural differences among the same genus, two additional collections, already identified as *Lithothamnion minervae* (Basso, 1995) and *Lithothamnion valens* Foslie 1909 have been considered. These collections have

90 been sampled alive from Egadi Islands (Italy), during July 2016, at 103 and 86 m of water depth respectively.

All samples have been air dried, sheltered from sunlight. Once dried, they have been stored in plastic boxes with silica to avoid any decay and transported to the laboratories of the University of Milano-Bicocca.

The seawater temperature has been extracted by 11 years of monthly reanalysis spanning 1979-2017 from ORAS5 (Ocean ReAnalysis System 5), at 0.25-degree horizontal resolution (Zuo et al., 2019), to indicate the seasonal temperate fluctuation

95 (Table 1)

2.1 Coralline sample preparation

Samples have been prepared for Scanning Electron Microscope (SEM) imaging. Altered, badly preserved or encrusted branches have been discarded. Only the branches showing a shiny surface have been picked from all collections, singly controlled under a Stereo Microscope, and cleaned manually by removing epiphytes and other incrustations. Each sample,

composed of multiple branches, has been cleaned in an ultrasonic bath in distilled water for 10 minutes and air-dried. The branches were then placed in small cylindrical plastic boxes with a base diameter of 1". Branches have been piled up and aligned to obtain multiple layers. The samples were embedded in Epofix resin for SEM analyses, which was stirred for 2 minutes with a hardener (13% w/w), and they were left to harden for one day at room temperature. Samples have then been cut normal to the multiple layers by using a IsoMet diamond wafering blade 15HC, along the direction of branch growth. The number of branches *per* sample are indicated in Table 1. Moreover, two additional samples have been prepared for SEM observation (n = 10 branches), by breaking them with a small chisel. Both longitudinal and surface sections have been selected for SEM observations.

2.2 Scanning Electron Microscope

For SEM imaging, the surfaces of embedded samples have been polished by using different sizes of silicon carbide, cleaned ultrasonically in distilled water for 10 minutes and air-dried. Samples mounted directly on stub have been simply chrome-coated. SEM images have been taken with a Field Emission Gun Scanning Electron Microscope (SEM-FEG) Gemini 500 Zeiss, and a Tescan VEGA TS 5136XM. Standard magnification for SEM images were established (~2500X, ~5000X, ~10000X, ~20000X and ~30000X), to describe comparatively and measure growth bands and cells, the morphology of Mg-calcite crystals, and the main features of perithallial and epithallial cell walls. A rigorous control over cell orientation is required to represent, describe, and measure in 2D the main features of a 3D structure such as cell calcification (both PW and SW). Longitudinal axial sections of branches are a standard representation for calcareous red algae, allowing for subsequent visual comparison (Woelkerling, 1988; Quaranta et al., 2007; Burdett et al., 2011). Surface tangential sections are useful to describe the epithallial cells. Transverse or oblique sections are useful to describe qualitatively the three-dimensional aspects and organization of calcite crystals composing both PW and SW. Description of the cell wall structure follows the nomenclature of Flajs (1977), presenting the primary (PW) and secondary (SW) calcifications of the wall. Some authors refer to PW as interstitial calcite (Ragazzola et al., 2016) or interfilament calcite (Nash and Adey, 2017; Nash et al., 2013, 2015). Cell dimensions have been measured as reported in Figure 2 (n=10 *per* sample), exclusively on longitudinal sections (Fig. 2). Separation among adjacent filaments was not always obvious (Fig. 2c). In such cases, PW of adjacent cells has been measured in total (green line in Fig. 2c) and then half of the total was attributed to each cell. In the text we use the term *ultrastructure* to identify the singular crystal into specific layer of the cell wall, and *ultrastructural pattern* to indicate the combination and mutual organization of crystals in layers of cell wall.

2.3 Statistical analyses

Spearmen and Pearson's correlations were used to test the statistical relationship between the cell measurements in both long and short cells, including morphometry and cell wall thickness. The linear correlation between the mean cell lengths and the sampling depths was measured by Pearson's coefficient, as well. One-way ANOVA and the Kruskal-Wallis test respectively followed by the Tukey's test and the Dunn's test for post-hoc analysis was used to compare the cell measurements among

sampling sites and to evidence the differences between group means and medians. All statistical analyses were run in R 3.6.3 software.

2.4 Growth rates

135 Growth rates were estimated under light microscope by measure a linear transect on the longitudinal section and counting how many growth-bands of fourth order *sensu* Foster (2001) intercept. The growth-rate has been calculated by dividing the measure for the number of growth-band.

3. Results

3.1 Ultrastructures from SEM images

140 Selected rhodoliths belong to the unattached branches morphotype (Basso, 1998; Basso et al., 2016), never exceeding 3 cm in length (Fig. 1). The diameter of each branch never exceeds 2.5 mm (Fig. 1). The color varies from yellowish white to pink/purplish, with typical knob-like apices (Fig. 1).

Once cut, all samples show the same micromorphology (Fig. 3a-i), with the constant occurrence of an easily detectable banding due to the alternation of series of short and long cells (Fig. 3a, b) in bands of the fourth order corresponding to 1 year (Foster,

145 2001). No reproductive structure (conceptacle) was detected.

Along the perithallus, long cells are ovoid to rectangular in shape (Fig. 3c, d), whereas short cells are more squared (Fig. 3e, f).

Within the long-celled bands, the longest cells were measured in the sample from Morlaix Bay (26.71 ± 1.74 µm), while the less elongated cells were observed in the sample from the Pontine Islands (13.05 ± 0.76 µm) (Table 2, Fig. 4).

150 Within the short-celled bands, the shortest cells were observed in the sample from Pontine (6.97 ± 0.25 µm), while the longest short cells were from Morlaix Bay (13.90 ± 0.88 µm) (Table 2, fig. 4). Cell diameter ranges between 7.69 ± 1.07 µm (Santa Caterina shoal) and 11.11 ± 1.79 µm (Morlaix) in long cells, and between 8.27 ± 0.48 µm (Pontine) and 9.23 ± 0.70 µm (Egadi) in short cells (Table 2, Fig. 4).

Both long and short cells have PW and SW walls, and the style of mineralization shows a consistent ultrastructural pattern.

155 The PW crystallization observed in longitudinal medial sections (cutting the cell lumen) is composed of elongated crystals appearing as rods (Fig 5a-c, e), but where longitudinal sections are tangential to the PW, crystals reveal to be flat rectangular tiles (Figs. 5d, f, 6a). The long axis of the PW tiles is parallel to the cell membrane and may form a multi-layered structure, which envelops the cell (Fig. 5e). The dimensions of the tiles are 0.61 ± 0.17 µm in length and 0.05 ± 0.01 µm in height (Fig. 6a). Elongated radial crystals (Fig. 7a, b) in longitudinal sections cutting the cell lumen characterize the SW. Small, roundish

160 crystals appearing as fused together, in places showing an apparent multi-layered structure (Fig. 7b) form such crystals. These elongated crystals are radial to the cell lumen (Fig. 7a-c). Where the cell membrane is lost, SW can be observed from different orientations, and such apparently elongated crystals reveal to be thin bricks with rounded margins (Figs. 6b, 7d-f). Bricks are squared, and length and width are 0.63 ± 0.15 µm (Fig. 6b). The bricks form a sort of envelope around the cell (Figs. 6b, 7e, f) showing sometimes a zigzag pattern (Fig. 7g, h).

165 Different thicknesses characterize PW and SW of short and long cells (Figs. 3, 5, 7; Table 2) in longitudinal medial sections. Both PW and SW of short cells are generally thicker than in long cells (Table 2), even if the thickness does not show a correlation with sampling bathymetry. SW thickness ranges between 1.52±0.65 µm (Pontine) and 2.20±0.45 µm (Elba) in short cells, and between 0.57±0.14 µm (Morlaix) and 1.26±0.42 µm (Santa Caterina shoal) in long cells (Table 2).

Both PW and SW show fibrils (Borowitzka, 1982) forming a dense network in support of the mineralization (Fig. 7d).

170 Epithallus is formed by one up to three flared cells in longitudinal sections (Figs. 3g-j, 5f, 7c), always mineralized, with some exceptions in the top distal surface (Fig. 3 g-j). The cell wall shows the same ultrastructural features of the perithallial cells, with both PW and SW mineralized (Figs. 3i, j, 5f, 7c).

Basing upon image analysis and time of collection, the calculated growth-rate ranges from 0.10 mm/yr in Pontine to 0.13 mm/yr in both Morlaix and Egadi.

175 The two additional collections, *L. valens* and *L. minervae* (Fig. 8), are characterized by both PW and SW (Fig. 8a, b, e, f). This last shows, in both cases, an ultrastructural arrangement like the one described for *L. corallioides* collections, with differently oriented bricks with rounded margins only apparently elongated and radial to the cell lumen in longitudinal sections (Fig. 8b, f). If observed into the cell lumen, where the cell membrane is lost, SW shows bricks with different orientation and sometimes a zigzag pattern (Fig. 8d, g).

180 On the contrary, PW shows a different shape and arrangement of crystals, which are not characterized by the tiles of *L. corallioides* observed in Figures 5d and 6a. Calcite crystals are squatter and more granular (Fig. 8a) or with irregular shape (Fig. 8h). One interesting aspect is that both samples show the occurrence of secondary calcite in form of dogtooth crystals filling the cell lumen (Fig. 8b, c, e).

3.2 Statistical analyses on morphological parameters

185 The differences in the long cells' morphometry and wall thickness among sampling sites are statistically significant for each measured parameter (p<0.05; Supplement 1) (Fig. 9). Interestingly, the long-cell length of the deepest sample from Pontine Isl. (66 m depth) is lower than the others (p<0.001) (Figs. 4, 9; Supplement), while in the shallowest sample collected in Morlaix (12 m depth) cells are notably longer (p<0.001) (Figs. 4, 9; Supplement 1).

In short cells, remarkable differences result only for cell (Fig. 9) and lumen lengths, and cell PW (p<0.05; Supplement). The
190 shortest cells are observed again in the sample from Pontine Isl., differing from the one collected in Morlaix (p<0.01) (Fig. 9; Supplement 1), which outstands for the highest values. On the contrary, the cell diameter slightly varies among sites, showing significant differences just in long cells (p<0.01; Supplement 1) (Fig. 9), with significantly higher values in Morlaix with respect to Elba Island and Santa Caterina. The dimensions of the cell lumen change accordingly, because of the positive correlation with the cell dimensions (Supplement 1).

195 Although banding is reported for all samples, elongation decreases with increasing depth, showing a strong inverse correlation in long cells (p<0.01; r=0.98) (Fig. 9). The same trend is also observed in short cells, even with non-significant values (p=0.09) (Fig. 9).

4 Discussion

Properly oriented longitudinal and transverse/oblique sections are mandatory to obtain a precise comparative description of the main morphological features of CCA. Multi-scale approaches are also relevant, among which the ultrastructural pattern may represent a new powerful and strategic diagnostic tool (Figs. 3-7).

Recent studies based upon genetic identification exclude the occurrence of other *Lithothamnion* species in the maerl of Morlaix Bay (Carro et al. 2014; Melbourne et al., 2017). Based upon this identification and considering the macroscopic features, thallus pattern, microanatomy, morphology, and morphometry of cell walls (Figs. 3, 5-7, Table 2) we identified the samples from Morlaix Bay as belonging to the species *L. corallioides*.

We compared the Mediterranean specimens with the Atlantic *L. corallioides*, and upon corresponding morphology, anatomy, and ultrastructure (Figs. 3, 5-7, Table 2), we considered them as conspecific.

The perithallus of *L. corallioides* clearly shows the alternation of growth band of third and fourth orders (Fig. 3a, b), in agreement with Foster (2001). Fourth order bands represent the annual cycling, whereas third order ones represent seasonal variations and can be firstly distinguished by an evident chromatic change due to the different calcification thickness between long and short cells (Foster, 2001). In our samples, banding (third and fourth orders) is easily recognizable (Fig. 3), and both long and short cells length decrease across depth (Figs. 4, 9), as expected, mirroring a decrease in growth-rate, whereas diameter variation is significatively lower (Fig. 4, Supplement 1).

Giraud and Cabioch (1979) observed that a cell wall fracture in *L. corallioides* shows a layer of radial calcite crystals (SW) separated from its neighbor by a different sheet composed of tangential crystals (PW). A discontinuity that coincides with the fibrillar matrix observed in sections of decalcified material marks the limits of adjacent cellular frames (Giraud and Cabioch, 1979). Our results match with the observation of these authors in longitudinal sections (Figs. 3, 5, 7), although the discontinuity between adjacent cells is not easily detectable because of the total mineralization.

Auer and Piller (2020) built a morphological tree based upon the observation of different ultrastructural patterns in epithallial cells, which match with the phylogenetic tree at family level. For Hapalidiaceae, and in the *Lithothamnion*-type epithallial ultrastructure, they observed the occurrence of PW with primary crystals formed along the middle lamella and the SW with secondary rod-shaped crystals, also presenting fan-like structures. The samples studied in the present work show PW and SW both in perithallial and epithallial cell walls (Figs. 3, 5, 7). Both are composed of apparently rod-like crystals in longitudinal sections. However, on longitudinal sections that are locally tangential to the PW, the apparent rods reveal to be the longest and thinnest side of variably oriented rectangular tiles (Figs. 5, 6a). The tiles that envelop the cell (Fig. 5d, f) are the basic ultrastructural elements forming the PW. Differently, apparent rods of the SW reveal to be squared and relatively flat bricks with rounded margins as observed at the cell lumen without membrane or exactly at the contact between SW longitudinal section and cell lumen (Figs. 6b, 7). Crystals in longitudinal sections of SW are radial to the cell lumen, in agreement with Giraud and Cabioch (1979), and seem formed by small grains fused together (Figs. 3, 7b, f). They can also show a zigzag pattern (Fig. 7g, h) like the fan-delta structure described by Auer and Piller (2020).

Therefore, our findings agree with the results of Auer and Piller (2020), although providing a more precise description of the ultrastructural pattern of *L. corallioides* (Fig. 6).

Despite the different environmental conditions, likely occurring at the different sampling sites and depths, the ultrastructures of both PW and SW seem conservative and detectable in all samples. Therefore, the ultrastructures and the ultrastructural pattern is not dependent on environmental controls.

However, *L. corallioides* shows variable cell elongations (Table 2) and growth-rates, decreasing both with according to sampling depth (Fig. 9), and a variation in PW and SW thickness, generally major in short than in long cells, not-dependent on depth (Table 2, Supplement 1). These features possibly represent the effect of the different environmental conditions in which it lives, but without affecting the ultrastructural pattern.

As defined by Lowenstam (1981), in the controlled biomineralization process organisms have extensive control over the mineral formation and it results in well-ordered mineral structures with minor size variations and species-specific crystal habits, as we detected in *L. corallioides*. Despite some analogies with the observation of Nash et al. (2019), our findings support that biomineralization process in CCA is biologically-controlled (Borowitzka, 1984; Cabioch and Giraud, 1986), rather than induced (de Cervalho et al., 2017; Nash et al., 2019). The two additional samples, *L. minervae* and *L. valens*, show distinct styles of PW calcification, and this is extremely interesting for its application in Paleontology. Ultrastructures and ultrastructural pattern possibly represent a powerful tool for morphological species identification. Further investigation is needed to clarify the validity of this hypothesis in other genera/species.

Finally, the occurrence of calcite in form of dogtooth crystals that fill the cell lumen (Fig. 8b, c, e) is an exceptional finding. The voids of the cell lumens allowed the development of calcite crystals which in term of shape, dimension and pattern are completely different from the original ones forming the cell wall calcification. It represents a form of extremely early alteration, possibly diagenesis, in collections that were alive at time of sampling. The phenomenon of early diagenesis has implications in the reliability of climate and paleoclimate studies based on the geochemistry techniques, also when applied to relative recent collections, as already indicated for Holocene Scleractinia corals (Nothdurft and Webb, 2008; Rachid et al., 2020). Therefore, the possible occurrence of dog-tooth calcite should be considered very carefully for coralline algae when selecting samples for this type of studies.

5. Conclusions

We define the cell-wall ultrastructural pattern of *L. corallioides* as follows:

- perithallus with evident banding as the result of the alternation of series of short-squared and long ovoid/rectangular cells;

- epithallus with one up to three flared cells;

- same and consistent ultrastructural pattern of the cell walls both in perithallus and epithallus, with PW and SW calcite walls always present;

- the PW is characterized by rectangular tiles;

- the SW is characterized by flattened squared bricks with roundish outlines;

- long and short cells have similar diameter, with different thickness of PW and SW, resulting mainly in a thicker PW and SW

265 in short cells.

The variable cell elongation, decreasing according to depth, and producing an evident banding, never affects the ultrastructural pattern that maintains the same arrangement also under different growth-rates. These findings support that the CCA calcification process seems to be biologically-controlled rather than induced. The comparison with other *Lithothamnion* species highlights difference in the mineralization pattern of PW. Therefore, the ultrastructures of the cell wall in CCA results

270 to be a promising new diagnostic tool for species identification with important potential application in Paleontology. Lastly, early alteration phenomenon, at the scale of ultrastructures, have been identified for the first time in living coralline algae.

Authors Contribution

Bracchi Valentina Alice conceived the research, conducted SEM observations, interpreted the results, and wrote and revised the manuscript. Basso Daniela conceived the research and wrote the manuscript. Piazza Giulia conducted the statistical

275 analyses.

Acknowledgments

We are grateful to two anonymous reviewers for their fruitful comments on the manuscript. Agostino Meroni is thanked for the extraction of temperature values. For the sample of Pontine islands: captain, crew and scientific staff of RV Minerva Uno cruise STRATEGIA MARINA LIGURE-TIRRENO are acknowledged for their efficient and skillful cooperation at sea.

280 Sample of Capo Carbonara has been collected in the framework of the agreement between the University of Milano-Bicocca and the Marine Protected Area of Capo Carbonara for the realization of the monitoring activities of Marine Strategy Framework Directive.

Giulia Piazza is funded by a doctoral fellowship in Earth Sciences of the Milano-Bicocca University.

This article is a contribution to the Project MIUR-Dipartimenti di Eccellenza 2018-2022 DISAT-UNIMIB.

285 **References**

Adey, W.H, and Mckibbin, D.L.: Studies on the Maerl Species *Phymatolithon calcareum* (Pallas) nov. comb. and *Lithothamnium corallioides* Crouan in the Ria de Vigo, Bot. Mar., 13(2), 100-106, doi:10.1515/botm.1970.13.2.100, 1970.

Adey, W.H.: Coralline algae as indicators of sea-level. In: van de Plassche O. (eds) Sea-Level Research. Springer, Dordrecht, doi:10.1007/978-94-009-4215-8_9, 1986.

290 Adey, W.H.: Review-coral reefs: algal structured and mediated ecosystems in shallow, turbulent, alkaline waters. J. Phycol. 34: 393-406, doi:10.1046/j.1529-8817.1998.340393.x, 1998.

Agnesi, S., Babbini, L., Bressan, G., Cassese, M.L., Mo, G. and Tunesi, L.: Distribuzione della Facies del Maerl e delle associazioni a rodoliti nei mari italiani: attuale stato delle conoscenze, Biol. Mar. Medit., 18(1), 50-51, 2011.

Aguirre, J., Riding, R., and Braga, J.: Diversity of coralline red algae: Origination and extinction patterns from the Early

295 Cretaceous to the Pleistocene. Paleobiology, 26(4), 651-667, doi:10.1666/0094-8373(2000)0262.0.CO, 2000.

Auer G., and Piller W.E.: Nanocrystals as phenotypic expression of genotypes - An example in coralline red algae Science Advance 6: eaay2126, 2020.

Basso, D.: Living calcareous algae by a paleontological approach: the genus *Lithothamnion* Heydrich nom. cons. from the soft bottoms of the Tyrrhenian Sea (Mediterranean), Riv. It. Pal. Strat., 101: 349-366, 1995.

300 Basso, D., Fravega, P., and Vannuci, G.: The taxonomy of *Lithothamnium ramosissimum* (Gümbel non Reuss) Conti and *Lithothamnium operculatum* (Conti) Conti (Rhodophyta, Corallinaceae), Facies, 37, 167-181, doi:10.1007/BF02537377, 1997.

Basso D., Nalin R., and Massari F. (2007). Genesis and composition of the Pleistocene Coralligène de plateau of the Cutro Terrace (Calabria, southern Italy). Neues Jahrbuch für Geologie und Paläontologie - Abhandlungen 244(2):173-182.

305 10.1127/0077-7749/2007/0244-0173

Basso, D., Babbini, L., Ramos-Esplá, A.A., and Salomidi M.: Mediterranean rhodolith beds. In: Rhodolith/maërl beds: A global perspective. Coas. Res. Lib., 15, 281-298. Springer, Cham, 2017.

Birkett, D.A., Maggs, C.A., and Dring, M.J.: An Overview of Dynamic and Sensitivity Characteristics for Conservation Management of Marine SACs, vol. 5. Maerl, Scottish Association for Marine Science, Scotland, 116 pp., 1998.

310 Blake, C., and Maggs, C.A.: Comparative growth rates and internal banding periodicity of maerl species (Corallinales, Rhodophyta) from northern Europe, Phycol., 42, 606–612, 2003.

Borowitzka, M.A.: Morphological and Cytological Aspects of Algal Calcification. Int. Rev. Cytol., 74, 127-162, 1982.

Borowitzka, M.A.: Calcification in aquatic plants. Plant, Cell & Environment, 7, 457-466, doi:10.1111/j.1365-3040.1984.tb01436.x, 1984.

315 Borowitzka, M.A., Carbonate calcification in algae - initiation and control. In: Mann S, Webb J, Williams RJP (eds) Biomineralization. Chemical and biochemical perspectives. VCH Verlagsgesellschaft, Weinheim, pp 63–95, 1989.

Bracchi, V.A., Nalin, R., and Basso, D.: Morpho-structural heterogeneity of shallow-water coralligenous in a Pleistocene marine terrace (Le Castella, Italy). Pal. Pal. Pal., 454, 101-112, 10.1016/j.palaeo.2016.04.014, 2014.

Bracchi, V.A., Nalin, R., and Basso, D.: Paleoecology and dynamics of coralline dominated facies during a Pleistocene
320 transgressive–regressive cycle (Capo Colonna marine terrace, Southern Italy). Pal. Pal. Pal., 414, 296-309, 10.1016/j.palaeo.2014.09.016, 2016.

Burdett, H., Kamenos, N.A., and Law, A.: Using coralline algae to understand historic marine cloud cover. Pal. Pal. Pal., 302(1-2), 65-70, 2011.

Cabioch, J., and Giraud, G.: Structural aspects of biomineralization in the coralline algae (calcified Rhodophyceae). In:
325 Leadbeater BSC, Riding R (eds) Biomineralization in lower plants and animals. Clarendon Press, Oxford, pp 141–156, 1986.

Caragnano, A., Colombo, F., Rodondi, G., and Basso, D.: 3-D distribution of nongeniculate corallinales: a case study from a reef crest of South Sinai (Red Sea, Egypt). Coral Reefs, 28(4), 881-891, 2009.

Carro, B., Lopez, L., Peña, V., Bárbara, I., and Barreiro, R.: DNA barcoding allows the accurate assessment of European maerl diversity: a Proof-of-Concept study. Phytotaxa, 190, 176-189, 2014.

330 de Carvalho, R.T., Salgado, L.T., Amado Filho, G.M., Leal, R.N., Werckmann, J., et al.: Biomineralization of calcium carbonate in the cell wall of *Lithothamnion crispatum* (Hapalidiales, Rhodophyta): correlation between the organic matrix and the mineral phase. J. Phycol., 53, 642-651, doi: 10.1111/jpy.12526, 2017.

Flajs, G.: Skeletal structures of some calcifying algae. E. Flügel (Ed.), Fossil Algae: Recent Results and Developments, Springer Berlin Heidelberg, pp. 225-231, 1977.

335 Foster, M.: Rhodoliths: between rocks and soft places. J. Phycol., 37, 659-667, 2001.

Gambi, M.C., Buia, M.C., Massa-Gallucci, A., Cigliano, M., Lattanzi, L., and Patti, F.P.: The "pink mile": benthic assemblages of rhodolith and maërl beds (Corallinales) off the Island of Ischia (Tyrrhenian Sea). In: C. Percent-Martini & M. Brichet (eds), UNEP-MAP-RAC/SPA, Proceedings of the 1st Mediterranean Symposium on the Conservation of the Coralligenous and Other Calcareous Bio-concretions (Tabarka, 15-16/1/2009): 198–201, 2009.

340 Giraud G., and Cabioch, J.: Aspects ultrastructuraux de la calcification chez les Corallinacées (Rhodophycées). J. Microscopie 26, 14a, 1976.

Giraud, G., and Cabioch, J.: Ultrastructure and elaboration of calcified cell-walls in the coralline algae (Rhodophyta, Cryptonemiales). Biologie cell 36(1), 81-86, 1979

Halfar, J., Zack, T., Kronz, A. and Zachos, J.C.: Growth and high-resolution paleoenvironmental signals of rhodoliths
345 (coralline red algae): A new biogenic archive. J. Geophys. Research-Oceans 105, 22107–22116, 2000.

Henrich, R., Freiwald, A., Betzler, C., Bader, B., and Schäfer, P.: Controls on modern carbonate sedimentation on warm-temperate to arctic coasts, shelves, and seamounts in the Northern Hemisphere: Implications for fossil counterparts. Facies 32:71–108, doi:10.1007/BF02536865, 1995.

Hernandez-Kantun J.J., Hall-Spencer J.M., Grall J., Adey W., Rindi F., et al.: North Atlantic Rhodolith Beds. In: Riosmena-
350 Rodríguez R., Nelson W., Aguirre J. (eds) Rhodolith/Maërl Beds: A Global Perspective. Coastal Research Library, 15. Springer, Cham, doi:10.1007/978-3-319-29315-8_10, 2017.

Huvé, H.: Contribution à l'étude des fonds à *Lithothamnium* (?) *solutum* Foslie (=*Lithophyllum solutum* (Foslie) Lemoine) de la région de Marseille. Recueil des Travaux de la Station Marine d'Endoume, 18, 105-133, 1956.

Irvine, L.M., and Chamberlain, Y.M.: Seaweeds of the British Isles. Vol. 1. Rhodophyta Part 2B Corallinales,
355 Hildenbrandiales. HMSO, London, 1994.

Jacquotte, R.: Étude des fonds de maërl de Méditerranée. Recueil des Travaux de la Station Marine d'Endoume: 141-235, 1962.

Kamenos, N.A., and Law, A.: Temperature controls on coralline algal skeletal growth. J. Phycol., 46, 331-335, 2010.

Lowenstam, H. A.: Mineral formed by organism. Science, 211, 1126-1131, 1981.

360 Melbourne, L.A., Hernández-Kantún, J.J., Russell, S., and Brodie, J.: There is more to maerl than meets the eye: DNA barcoding reveals a new species in Britain, *Lithothamnion erinaceum* sp. nov. (Hapalidiales, Rhodophyta), Eur. J. Phycol., 52(2): 166-178, doi:10.1080/09670262.2016.1269953, 2017.

Nash, M.C., and Adey, W.: Multiple phases of mg-calcite in crustose coralline algae suggest caution for temperature proxy and ocean acidification assessment: lessons from the ultrastructure and biomineralization in *Phymatolithon* (Rhodophyta,
365   Corallinales). J. Phycol., 53(5),970-984, doi:10.1111/jpy.12559, 2017.

Nash, M.C., Opdyke, B.N., Troitzsch, U., Russell, B.D., Adey, W.H., et al.: Dolomite-rich coralline algae in reefs resist dissolution in acidified conditions, Nat. Clim. Change, 3(3), 268-272, 2013.

Nash, M.C., Russell, B.D., Dixon, K.R. Liu, M., and Xu, H.: Discovery of the mineral brucite (magnesium hydroxide) in the tropical calcifying alga *Polystrata dura* (Peyssonneliales, Rhodophyta). J. Phycol., 51(3), 403-4077, doi:/10.1111/jpy.12299
370   PMID: 26986657, 2015.

Nash, M.C., Diaz-Pulido G., Harvey A.S., and Adey W.: Coralline algal calcification: A morphological and process-based understanding. PLoS ONE 14(9): e0221396, doi:10.1371/journal.pone.0221396, 2019.

Nothdurft, L.K, and Webb, H.E.: Earliest diagenesis in scleractinian coral skeletons: implications for palaeoclimate-sensitive geochemical archives, Facies, 55, 161-201, doi:10.1007/s10347-008-0167-z, 2008.

375   Peña, V., and Bárbara, I.: Maerl community in the north-western Iberian Peninsula: a review of floristic studies and long-term changes. Aq. Cons.: Mar. Freshw. Ecos., 18, 339-366, 2008.

Peña, V., and Bárbara I.: Distribution of the Galician maerl beds and their shape classes (Atlantic Iberian Peninsula): proposal of areas in future conservation actions. Cahier Biol. Mar., 50(4), 353-368, 2009.

Peña, V., Bárbara, I., Grall, J., Maggs, C.A., and Hall-Spencer, J.M.: The diversity of seaweeds on maerl in the NE Atlantic.
380   Mar. Biodiv., 44, 533-551, doi:10.1007/s12526-014-0214-7, 2014.

Potin, P., Floch, J.Y., Augris, C., and Cabioch, J.: Annual growth rate of the calcareous red alga *Lithothamnion corallioides* (Corallinales, Rhodophyta) in the Bay of Brest, France. Hydrobiologia, 204–205(1). https://doi.org/10.1007/BF00040243

Quaranta F., Vannucci G., Basso D. (2007). *Neogoniolithon contii* comb. nov. based on the taxonomic re-assessment of Mastrorilli's original collections from the Oligocene of NW Italy (Tertiary Piedmont Basin). Riv. It. Paleont. Strat., 113, 43-
385   55, 1990.

Ragazzola, F., Foster, L.C., Jones, C.J., Scott, T.B., Fietzke, J., et al.: Impact of high CO2 on the geochemistry of the coralline algae *Lithothamnion glaciale*. Scientific Report 6, 20572, 2016.

Ragazzola, F., Caragnano, A., Basso, D., Schmidt, D.N., and Fietzke, J.: Establishing temperate crustose early Holocene coralline algae as archives for paleoenvironmental reconstructions of the shallow water habitats of the Mediterranean Sea.
390   Palaeont., 63, 155-170, 2020.

Rashid, R., Eisenhauer, A., Liebetrau, V., Fietzke, J., Böhm, F. et al.: Early Diagenetic Imprint on Temperature Proxies in Holocene Corals: A Case Study from French Polynesia. Front. Earth Sci. 8:301, doi: 10.3389/feart.2020.00301, 2020.

Ries, J.B.: Mg fractionation in crustose coralline algae: Geochemical, biological, and sedimentological implications of secular variation in the Mg/Ca ratio of seawater. Geoc. Cosmoch. Acta, 70(4): 891-900, 2006.

395   Savini, A., Basso, D., Bracchi, V.A., Corselli, C., and Pennetta, M.: Maerl-bed mapping and carbonate quantification on submerged terraces offshores the Cilento peninsula (Tyrrhenian Sea, Italy). Geodiversitas, 34 (1), 77-98. http://dx.doi.org/10.5252/g2012n1a5, 2012.

Steller, D.L., Hernández-Ayón, J.M., Riosmena-Rodríguez, R., and Cabello-Pasini, A.: Effect of temperature on photosynthesis, growth, and calcification rates of the free-living coralline alga *Lithophyllum margaritae*, Ciencias Marinas,

400   33, 441-456, 2007.

Vásquez-Elizondo, R.M., and Enríquez, S.: Light Absorption in Coralline Algae (Rhodophyta): A Morphological and Functional Approach to Understanding Species Distribution in a Coral Reef Lagoon. Front. Mar. Sci., 4. 10.3389/fmars.2017.00297, 2017.

Wilson, S., Blake, C., Berges, J.A., and Maggs, C.A.: Environmental tolerances of free-living coralline algae (maerl):

405   implications for European marine conservation. Biol. Cons., 120, 279-289, 2004.

Woelkerling, W.J.: The coralline red algae: an analysis of the genera and subfamilies of non-geniculate Corallinaceae. British Museum (Natural History) and Oxford University Press, London, UK. 268 pp., 1988.

Zuo, H., Balmaseda, M. A., Tietsche, S., Mogensen, K. and Mayer, M.: The ECMWF operational ensemble reanalysis–analysis system for ocean and sea ice: a description of the system and assessment, Ocean Sci., 15, 779–808, doi:10.5194/os-15-779-

410   685 2019, 2019.

Captions, Figures and Tables

Figures

Figure 1: Sampling sites (1-5) and images of selected samples. Service Layer Credits: Sources: Esri, GEBCO, NOAA, National Geographic, Garmin, HERE, Geonames.org, and other contributors Esri, Garmin, GEBCO, NOAA NGDC, and other contributors. Scale bar = 1 cm.
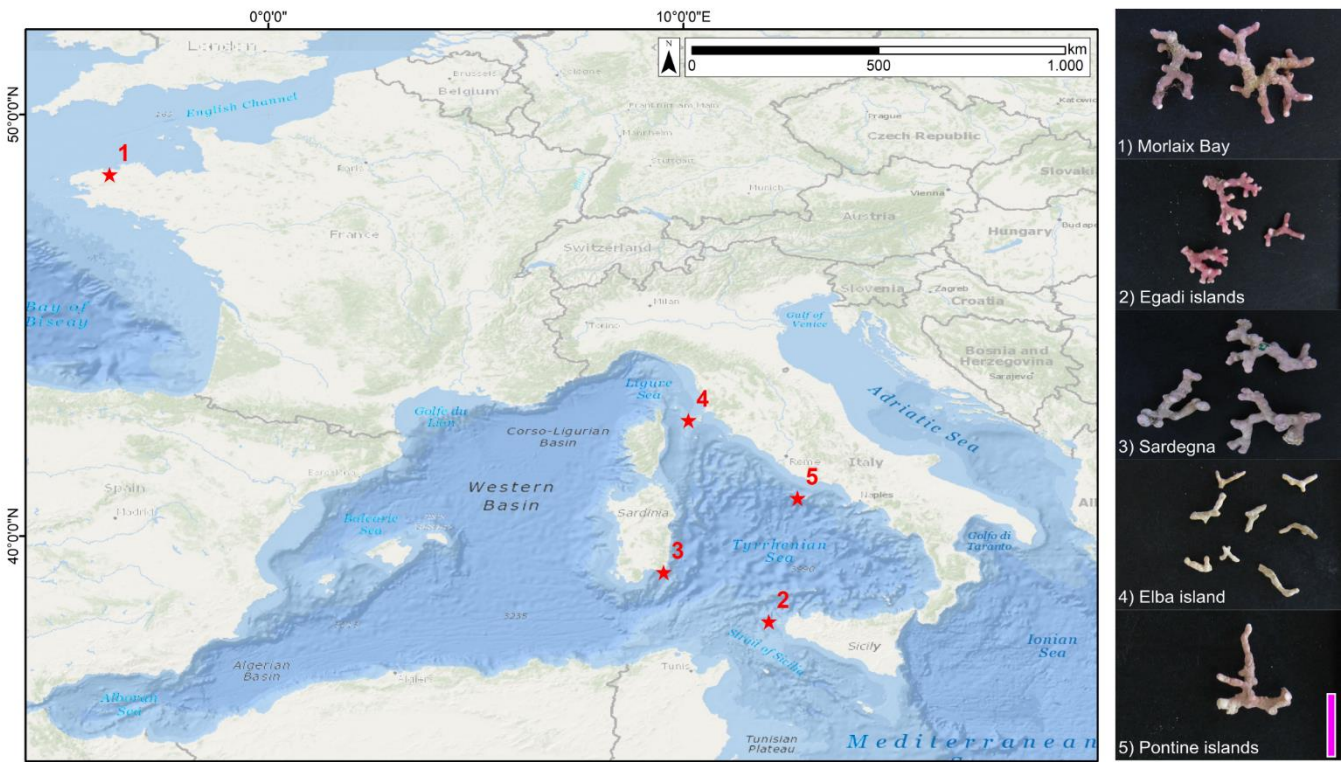
Figure 2: Cell measurement: a) cell wall length (red) and diameter (blue); b) lumen length (yellow) and lumen diameter (purple); c) SW thickness of adjacent cells (orange); PW thickness of adjacent cells (light blue).
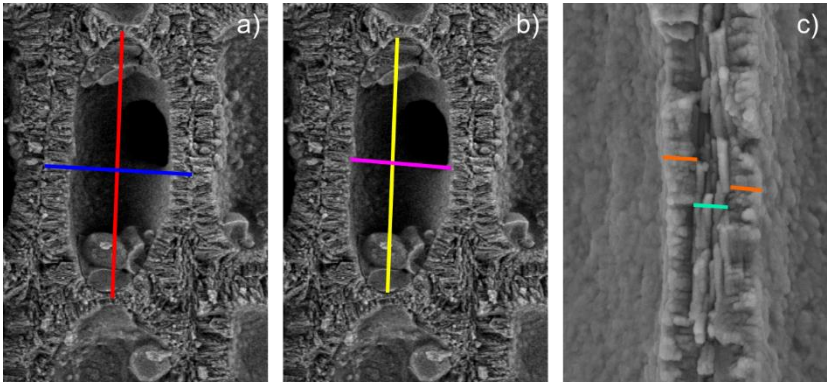
Figure 3: Main features of *Lithothamnion corallioides* under SEM (Morlaix Bay, France):

a) longitudinal section of a fragment of L. *corallioides* with obvious banding (black dashed lines). Scale bar = 100 µm. The inset is magnified in b). Scale bar = 100 µm;

b) alternation of thick-walled (black arrow) and thin walled (white arrow) cells. The inset is magnified in c). Scale bar = 20 µm;

c) Thin-walled long cells. The inset is magnified in d). Scale bar = 10 µm;

d) Detail of the thin wall of long cells. Scale bar = 1 µm;

e) thick-walled short cells. The inset is magnified in f). Scale bar = 2 µm;

f) detail of the thick wall of short cells. Scale bar = 1 µm;

g) polygonal shape of epithallial cells in surface view. Scale bar = 10 µm;

h) detail of a flared epithallial cell (arrow). Scale bar = 3 µm;

i-j) longitudinal sections of flared epithallial cells with complete mineralization of the cell walls. Scale bar = 2 µm.

435
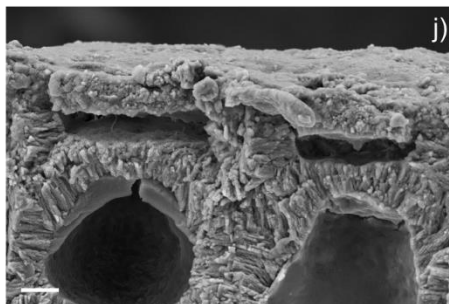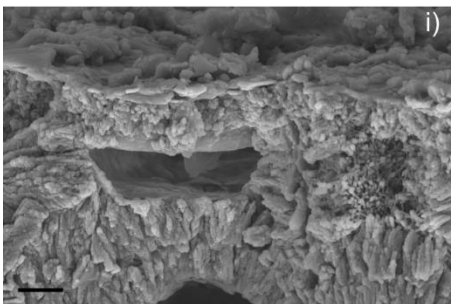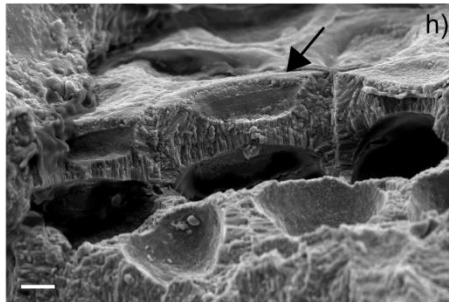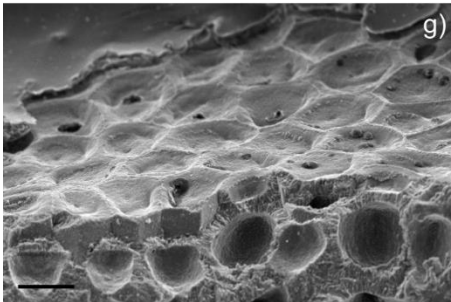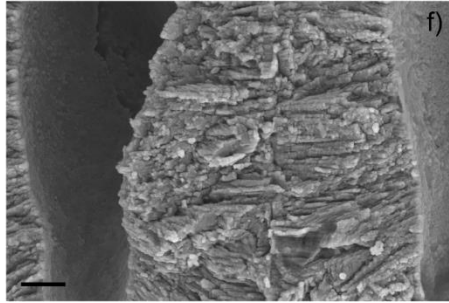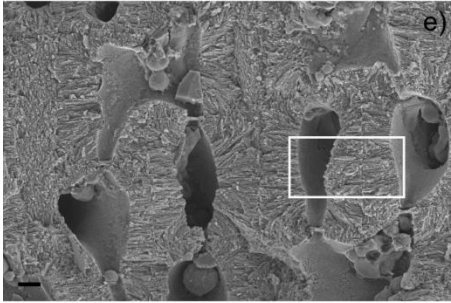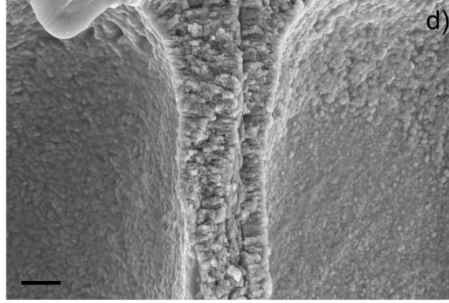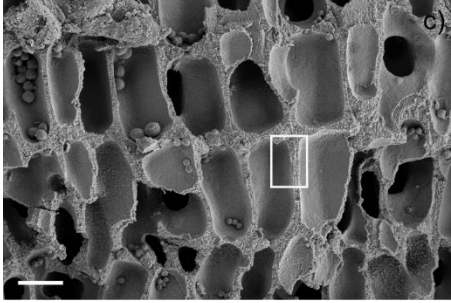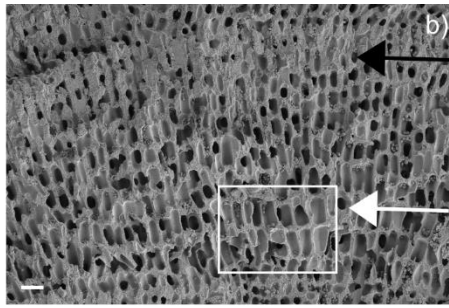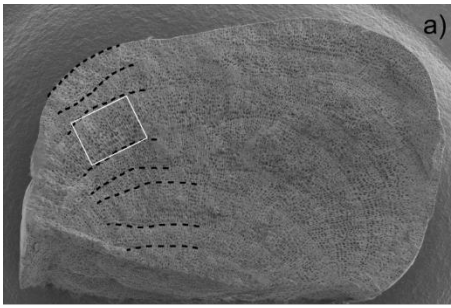
Figure 4: Box plots reporting cell lengths and cell diameters in both long and short cells of *L. corallioides* samples collected at different sampling sites, ordered along x-axis according to the depth.

440
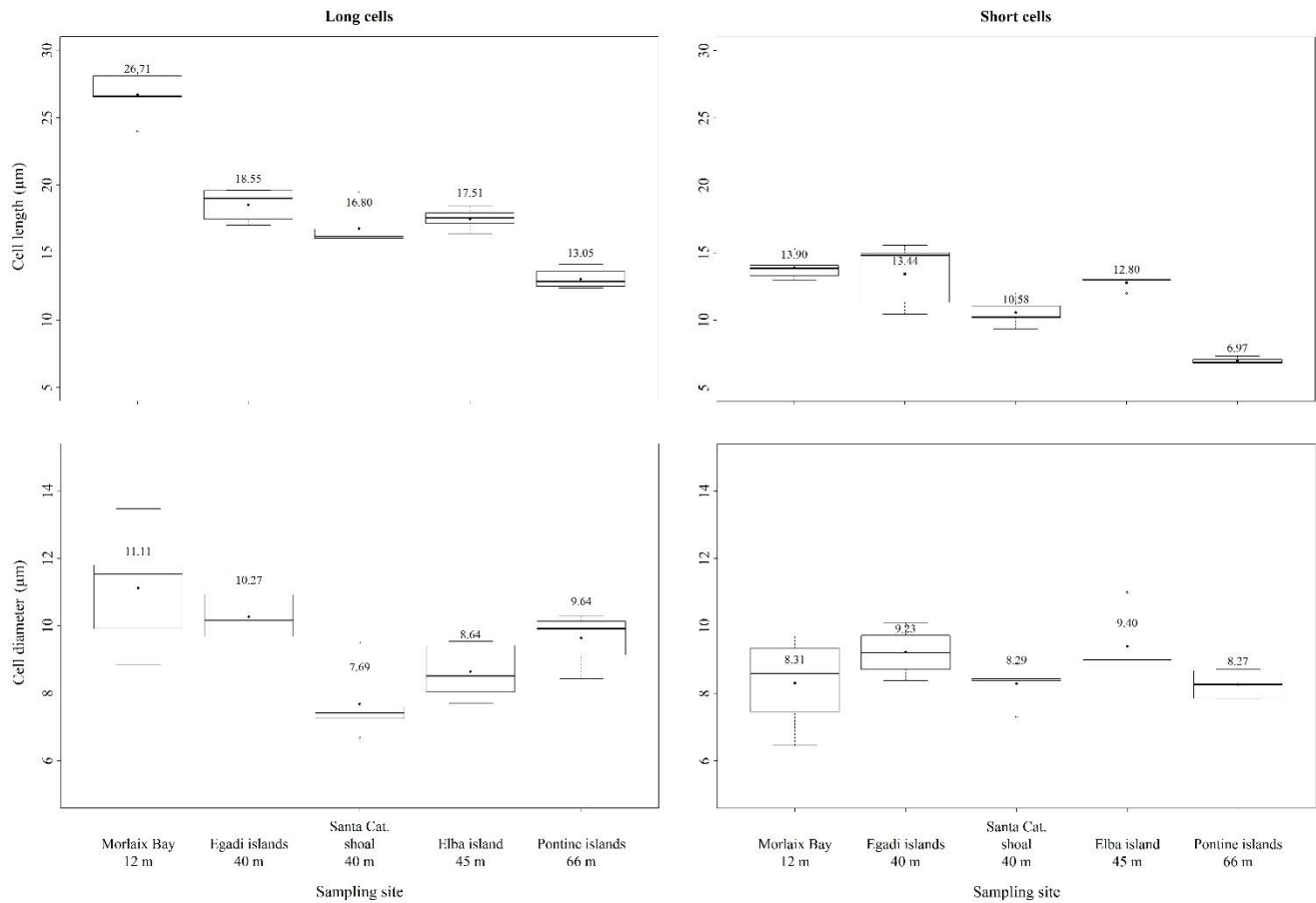
Figure 5: Details on primary wall (PW) in longitudinal section:

a) thick-walled short cell showing both PW (black arrow) and secondary wall (SW, white arrow), Santa Caterina shoal. Scale bar = 2 µm;

b) thick-walled short cell showing both PW (black arrow) and SW (white arrow), Pontine Islands. Scale bar = 2 µm;

c) thin-walled long cell showing both PW (black arrows) and SW (white arrow). PW crystals in longitudinal section appear as elongated crystals, Santa Caterina shoal. Scale bar = 1 µm;

d) thin-walled long cell showing both (black arrow) and SW (white arrow). The fracture shows detail of tiles composing the PW (black arrow), Santa Caterina shoal, scale bar = 1 µm;

e) details of multi-layered PW (black arrow) and SW (white arrows). PW crystals in longitudinal section appear as elongated crystals. Pontine Islands, scale bar = 0.2 µm;

f) perithallial and epithallial cells where the longitudinal section is locally tangential to the PW (black arrows): crystals appear as flat rectangular tiles, Santa Caterina shoal. Scale bar = 2 µm.
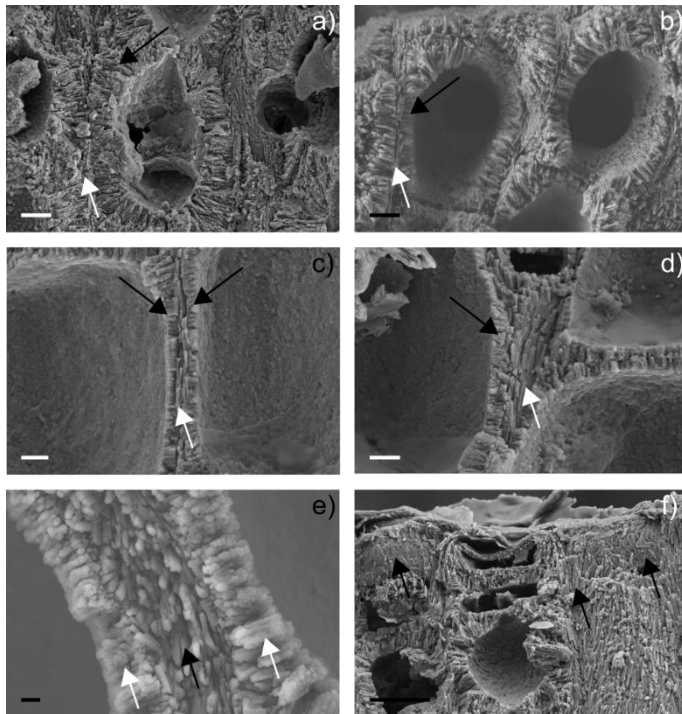
455   Figure 6: Ultrastructures of *Lithothamnion corallioides*: a) Rectangular tiles of the PW; b) squared bricks of SW.
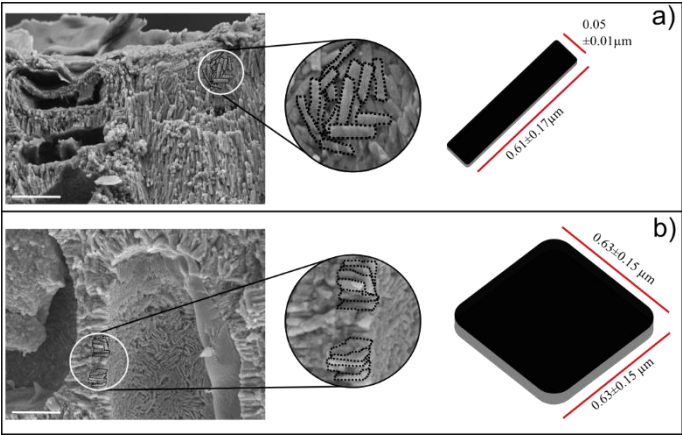
Figure 7: Details on secondary wall (SW) in longitudinal section:

a) thick-walled short cells SW showing both PW and SW, Morlaix Bay. Inset magnification in b). Scale bar = 2 µm;

b) Two adjacent cells with both PW and SW. The secondary wall is characterized by elongated radial crystals formed by small roundish crystals appearing as fused together, in places showing an apparent multi-layered structure. Note the occurrence of a very thin PW (black arrow). Morlaix Bay. Scale bar = 1 µm;

c) perithallial thick-walled short cells showing both PW and SW, and one-layer epithallial cell with the evidence of a flattened cell (red arrow), Morlaix Bay. Inset 1 magnification in d), inset 2 magnification in e) and inset 3 magnification in f). Scale bar = 2 µm;

d) magnification of inset 1 in c) showing SW in lumen cell with no membrane. In this view the crystals appear as ovoidal to rod-shaped with a complex orientation, associated with fibrils. Morlaix Bay. Scale bar = 1µm;

e) magnification of inset 2 in c) showing SW in lumen cell with no membrane. A section showing at the same time a longitudinal section and the inner cell reveal the actual 3D shape of the SW crystals that are thin bricks (white arrows). Morlaix Bay, scale bar = 1 µm;

f) magnification of inset 3 in c) showing SW in lumen cell with no membrane. A section showing at the same time a longitudinal section and the inner cell reveal the actual 3D shape of the SW crystals that are thin bricks (white arrows). Morlaix Bay, scale bar = 1 µm;

g) a detail of SW inside a cell lumen. The crystals are thin bricks with a complex zig-zag orientation. Inset magnification in h). Egadi Islands, scale bar = 2 µm;

h) a zigzag and/or crossing pattern of bricks in SW. Egadi Islands, scale bar = 1 µm.
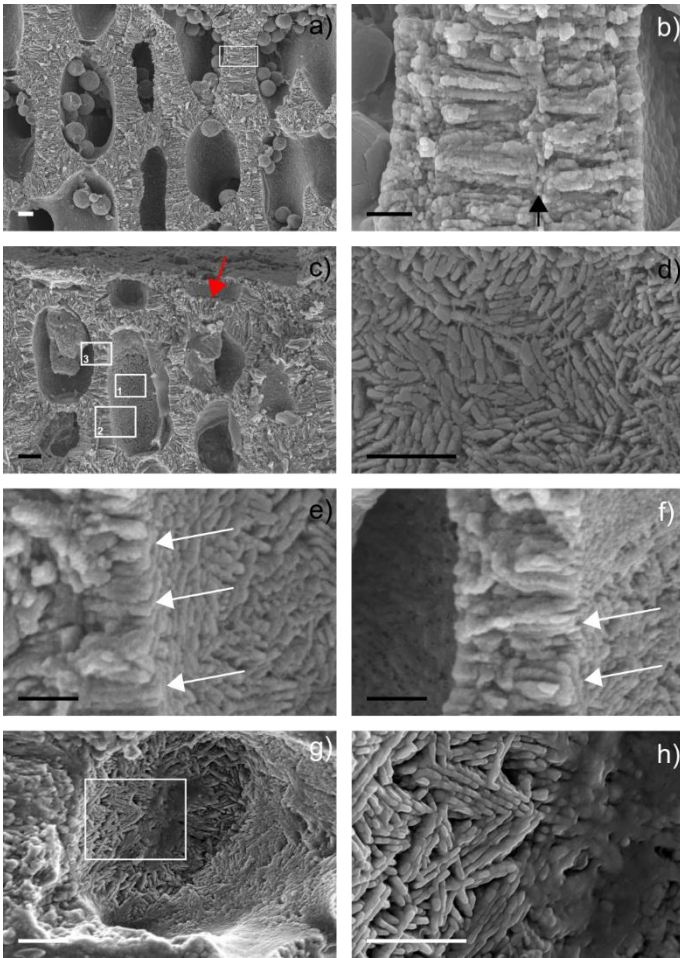
Figure 8: Details on the main ultrastructures of *Lithothamnion valens* (a-d) and *Lithothamnion minervae* (e-h):

480   a) perithallial and epithallial cells showing both PW and SW. Scale bar = 2 µm;

b) details of perithallial cell with both PW (yellow arrow) and SW (white arrow). The secondary wall is characterized by elongated radial crystals, whereas PW crystals are tangential to the cell lumen. The cell lumen is filled by secondary calcite (dogtooth shape, red arrows). Scale bar = 1 µm;

c) detail of a cell wall with evident PW (yellow arrow) and SW (white arrow), and secondary dogtooth calcite filling the cell

485   lumen (red arrow). Scale bar = 2 µm;

d) detail of SW (white arrow) into the cell lumen. Note the multi-direction arrangement of calcite crystals. Scale bar = 2 µm;

e) perithallial cell, with elongated and rectangular shape. The central cell shows a cell lumen filled by secondary calcite with dogtooth shape (red arrow). Scale bar = 2 µm;

f) perithallial cell with both PW (yellow arrow) and SW (white arrows). Note in the cell lumen that SW is characterized by

490   elongated crystals showing different orientation and fan-delta arrangement. Scale bar = 2 µm;

g) detail of f, with the SW into the cell lumen, with elongated crystal showing different orientation and fan-delta arrangement. Scale bar = 1 µm;

h) the fracture shows detail of crystals composing the PW (yellow arrow) apparently forming by granules. SW is characterized by elongated crystals in longitudinal section (white arrow). Scale bar = 1 µm.

495
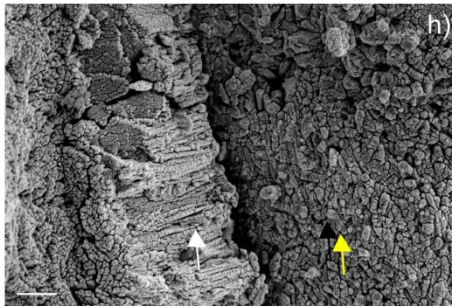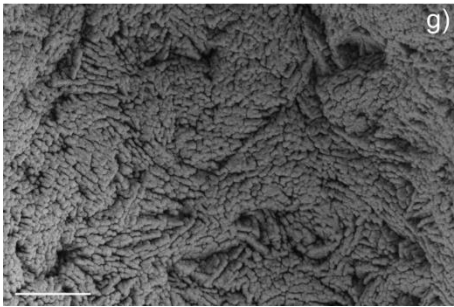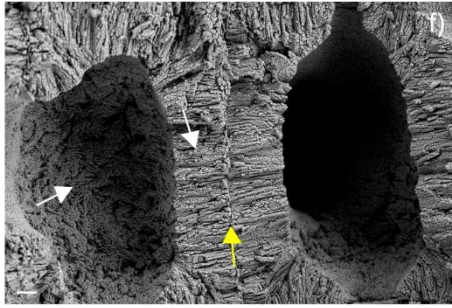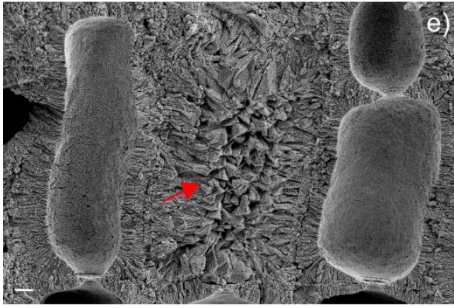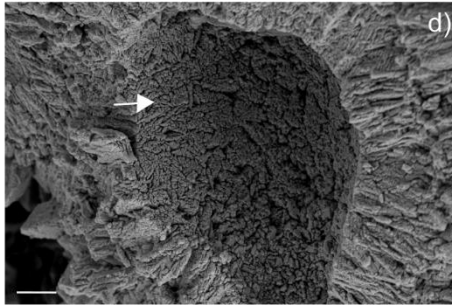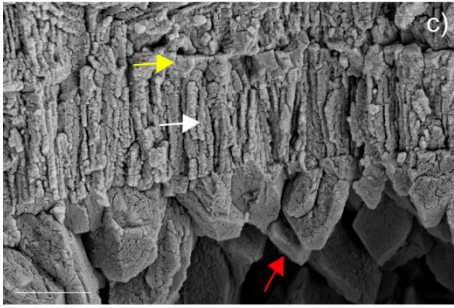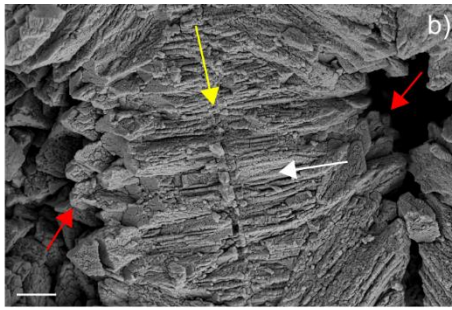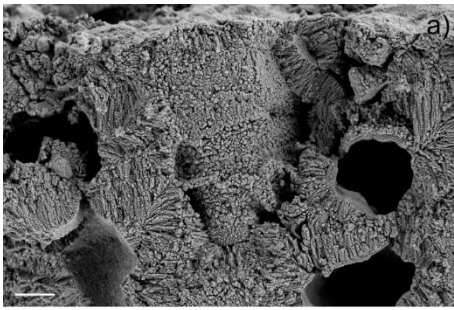
Figure 9: Correlation plots showing the relationship between sampling depth and cell lengths, measured in both long and short cells. Pearson's correlation significance at p<0.05. Pink is for Morlaix Bay (France, 12); green is for Egadi islands (Italy, 40); red is for Santa Caterina shoal (Italy, 40); yellow is for Elba Island (Italy, 45); Blue is for Pontine islands (Italy, 66).
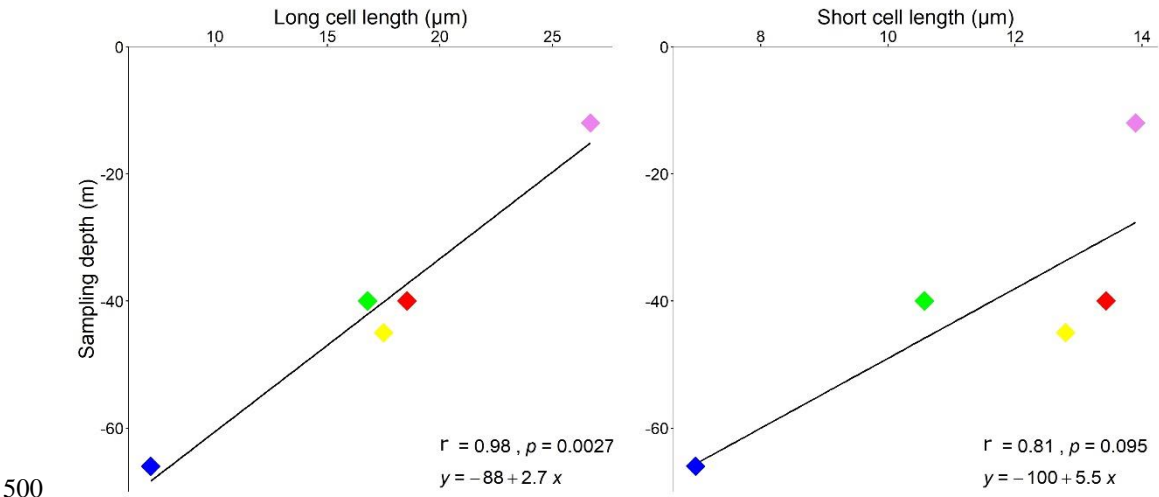
Tables

Table 1: Location, date of collection and depth of samples. In Basin column, numbers in brackets corresponds to the point in Figure 1.

Basin	Sample	Location	Date of collection	Depth (m)	n° branches	Temperature seasonal range (°C)
Atlantic Ocean (1)	France, Morlaix Bay	48°34′42″N 3°49′36″W	May, 1991	12	23	8.3-17.2
W Mediterranean (2)	Italy, Egadi Islands	37°58′10″N 12°03′26″E	August, 1991	40	20	13-7-18.8
W Mediterranean (3)	Italy, Santa Caterina shoal	39°08′32″N 9°31′14″E	July, 2017	40	12	13.2-20
W Mediterranean (4)	Italy, Elba Island	42°44′56.4″N 10°07′08.4″E	December, 1990	45	20	12.9-17.5
W Mediterranean (5)	Italy, Pontine islands	40°54'N 12°45'E	July, 2016	66	12	13.9-16.7

Table 2: Morphometry of short and long cells/lumens and wall thickness measured in longitudinal section (PW = primary wall, SW = secondary wall), with the indication of length (L) and diameter (D) (µm). Standard deviation in brackets.

Sample	Short cell						Long cell					
	Cell		Lumen		Wall		Cell		Lumen		Wall	
	L	D	L	D	SW	PW	L	D	L	D	SW	PW
Morlaix Bay 12 m	13.90 (0.88)	8.31 (1.34)	12.38 (0.93)	6.04 (1.05)	1.61 (0.43)	0.12 (0.03)	26.70 (1.73)	11.11 (1.80)	24.46 (1.73)	9.25 (1.42)	0.57 (0.14)	0.13 (0.06)
Egadi islands 40 m	13.43 (2.36)	9.22 (0.70)	8.48 (1.189)	4.97 (1.55)	2.08 (0.80)	0.22 (0.07)	18.55 (1.28)	10.27 (0.77)	16.13 (1.16)	8.54 (0.60)	0.74 (0.09)	0.16 (0.05)
Santa Cat. shoal 40 m	10.57 (1.01)	8.29 (0,58)	8.79 (0.72)	4.43 (0.66)	1.87 (0.26)	0.17 (0.16)	16.80 (1.54)	7.69 (1.07)	15.40 (1.51)	5.04 (0.81)	1.25 (0.41)	0.13 (0.03)
Elba island 45 m	12.8 (0.45)	9.4 (0.9)	11.6 (0.54)	5.2 (0.44)	2.2 (0.44)	0.14 (0.05)	17.51 (0.78)	8.64 (0.81)	15.75 (0.89)	6.31 (0.83)	1.08 (0.25)	0.18 (0.06)
Pontine islands 66 m	6.97 (0.25)	8.27 (0.47)	5.19 (0.72)	4.49 (0.31)	1.79 (0.27)	0.47 (0.08)	13.05 (0.76)	9.64 (0.83)	10.38 (0.54)	6.81 (0.87)	1.22 (0.17)	0.33 (0.09)